

Presented in:

The First International Conference on Computational Methods in  
Multiphase Flow

Conference preceding:

**Computational Methods in Multiphase Flow**

Editors:

H. Power and C.A. Brebbia

Publisher: WIT press, Southampton, Boston

Publication date: 2001

ISBN: 1-85312-862-7

ISSN: 1353-808x

## **Three-dimensional homogenous two-phase flow modelling of drifting sand around an open gate**

S. Al-Hajraf<sup>1</sup> & P. Rubini<sup>2</sup>

<sup>1</sup>*Kuwait Institute for Scientific Research (KISR), Kuwait*

<sup>2</sup>*School of Mechanical Engineering, Cranfield University, UK*

# Three-dimensional homogenous two-phase flow modelling of drifting sand around an open gate

S. Al-Hajraf<sup>1</sup> & P. Rubini<sup>2</sup>

<sup>1</sup>*Kuwait Institute for Scientific Research (KISR), Kuwait*

<sup>2</sup>*School of Mechanical Engineering, Cranfield University, UK*

## Abstract

This paper introduces a numerical model for two- and three-dimensional simulations of sand drifting. The model is based on a homogenous two-phase flow model, where the flow field is predicted by solving the Navier-Stokes equations for transient, incompressible, viscous flow in a general curvilinear coordinate system. The particle volume fraction is predicted by solving the **convection/diffusion** transport equation. The transport equations are discretized in a Eulerian reference frame using the Finite Volume method. Particles transported by suspension and saltation are both considered in the transport equation source term. An Erosion-Deposition algorithm is used to account for the transient change of the solid interface boundary, which is allowed to grow or erode according to the wind surface shear velocity and the particle volume fraction. The model is validated for both full-scale and wind tunnel measurements of particles accumulating at a solid wall. **Finally**, the model is employed to simulate a **full-scale** field experiment held in the Kuwaiti desert for sand accumulation at an open gate facing the prevailing wind. The results show that sand is deposited in regions of weak flow velocity around the gate. The model shows good quantitative results in comparison to observations.

## 1 Introduction

Wind blown particles (e.g. sand, snow or soil) occur as the result of a natural phenomenon known as an Aeolian process. The **Aeolian** process is divided into three stages, erosion, transportation and then deposition, commencing when the wind entrains a particle from rest and carries it for some distance. When the aerodynamic forces applied to a particle become less than the gravitational force,

the particle finally settles back to the ground, Bagnold [1], Tabler [2], Pye [3] and Iversen [4]. A large number of field and wind tunnel studies have been conducted to study the physical behaviour of wind blown particles as they approach obstacles of different shapes such as buildings, roads, farms, security fences, oil wells etc. However, field and wind tunnel experiments demand equipment, manpower and time, often at high cost. Therefore, with the continued development of numerical and physical models and the availability of powerful computational resources, the numerical simulation of multi-phase flows has, in recent decades, been applied to many engineering and environmental applications, Ishii [5], Gosman [6] and Manninen [7].

Drifting snow against obstacles of different shape has been studied numerically by many authors including for example, Kawamura [8], Uematsu [9] and Sundsbø [10]. Simulation of the emigration of sand dunes on flat surfaces has been modelled by Wipperman [11] utilising empirical formulation to predict the particle mass flow rate.

In this paper, a numerical model is presented, which incorporates physical models for both suspension and saltation in the transport equation for the particle volume fraction as individual contributions in the source terms. An erosion-deposition algorithm is described which allows the deposition of particles to form a solid interface boundary, changing shape and position as time passes. Equally, any previously deposited particles are allowed to be re-entrained whenever the specified erosion conditions are satisfied. The variation in time of the dune surface is modelled using a modified form of the Fractional Area-Volume Obstacle Representation technique (FAVOR) presented by Hirt [14]. The model is validated by comparing the predicted results with field experiments conducted as part of this study in the Kuwait desert. These were designed to investigate the pattern of deposition around a solid wall with an open gate facing the prevailing wind direction.

## **2 Field observations of drifting sand at a solid wall with an open gate**

Entrances and gates of farms, military bases, oil field installations and electricity transformation stations are examples of where drifting sand can cause daily problems by obstructing traffic or blocking camp entrances. The aim of the field study was to obtain natural sand deposition patterns around a full-scale gate to be used in the validation of the numerical model.

The study investigated the development of a sand dune at and around an open gate by placing two solid walls, 1.5m height 'H', 39m and 15m in length separated by a 4m gap. The study was conducted in an area lying within a desert region of high sand flow rate as shown from the satellite image in figure 1.

The emphasis of the trial was on the different stages of the sand accumulation process. Theoretically, under constant wind speed and direction, the steady state deposition profile can be achieved much faster under higher mass flow rate than that of lower flow rate, in both cases, the steady state deposition pattern must be identical. Thus the natural flow rate of sand particles was assumed to be unimportant and therefore the speed of the dune development process was enhanced by increasing the upstream flow rate reduce the time required to complete the process. To achieve this, a sand bed of 0.3-metre depth was spread over a 60m x 30m region upstream of the wall, figure 2, to enhance the particle mass flow rate.

A cross-sectional deposition profile was measured by placing 30 vertical beams of 2m height along the centreline of the 20m long wall, which were used as reference points for the measurements. The deposition height was measured by subtracting the height of the beam appearing above the ground from the original beam height. Figure 3, shows the deposition profiles at different times during the experiment. Similar to the observations from the previous field and wind tunnel experiments of drifting particles at solid wall, Tabler [2]. The deposition process started upstream from the wall with a dune crest at about 0.5H from the wall.

As the wind impinges upon the wall, the flow is divided into streamlines. The upper streamline is directed to flow over the top of the wall with a consequent increase in velocity. The lower streamline is directed downward generating a reverse flow zone in front of the wall. The strength of the resulting eddy is responsible for the location of the initial deposition process. A weak eddy results in the deposition process starting closer to the wall. As the eddy increases in size the initial deposition takes place at greater distances from the wall while the dune crest moves further upstream.

As the dune grows, the height of the dune crest increases and moves closer towards the wall until the dune becomes attached to the wall and then starts climbing it. Figure 4 shows a series of photographs, taken from an upstream viewpoint, of the trial site at successive times. The figure illustrates the different stages in the deposition process and the change in the shape and size of the dune as a function of the strength of the reverse flow.

It can be clearly seen that the vertical growth of the dune occurs at the sharp edge of the dune slip face. The crest of the dune is a stagnation point, at which the reverse flow meets the flow coming from the upstream direction. The stagnation point is characterised by low wind velocities, resulting in surface friction velocities below the particle threshold velocity, which locally increase the rate of deposition.

Near the gate and around the ends of the walls, the strength of the eddies is reduced in comparison to that at the centreline of the wall. This occurs as a result of the wind stream flowing around the ends of the walls reducing the strength of the reverse flow. As a result the dune crest moves closer to the wall near the ends

of the walls and in the gate centreline, producing a crescent like deposition shape, figure 4.

In addition, the wind velocity increases as the flow turns around the ends of the walls causing an increase in the friction velocity and consequently an increase in the rate of erosion in these areas. As shown in figure 5, particles are completely eroded from the region where the wind friction velocity exceeds the particle threshold velocity. **However**, in the centreline of the gate, some particles do settle where the friction velocity is less than the particle threshold velocity.

Downstream from the gate, figure 6, the wind streamlines diffuse in all directions causing a reduction in the momentum of the wind and therefore the capability of the wind to carry particles for further distances. This results in a circular shaped particle deposition area. The direction of the sand waves on the dune surface can also be used to indicate the wind direction in that area, demonstrating that the diffusion of the wind occurs in all directions. Also it may be concluded that a symmetrical dune will be formed if the wind flowing through the gate is symmetric and an asymmetrical dune shape otherwise, as in the case of this study.

### 3 Numerical model

In this study, the solid phase, i.e. the sand particles, was represented as a second continuum flow phase superimposed upon the primary phase, the air, as described by the conventional **Navier-Stokes** equations. A flow regime containing two or more flow phases of different physical properties could be treated as a multi-phase flow system, which can be solved numerically based on the theory for a multi-phase flow system, **Ishii** [5], **Manninen** [7]. However, considering the air as the continuous phase (carrier phase) and the particles as the discrete phase, the simplest two-phase flow model, known as the *Homogenous two-phase flow model*, was employed in this paper. The model assumes that the system is one way coupled, implying that particles are driven by the wind as a result of the drag forces, but that the wind does not lose any of its momentum used to transport the particles.

The conservation equations can be expressed in a general form as:

$$\underbrace{\frac{\partial(\rho\phi_i)}{\partial t}}_{\text{Rate of change in } \phi} + \underbrace{\frac{1}{V_f} \frac{\partial}{\partial x_j} (\rho u_j \phi_i A_{ff})}_{\text{Convection term}} = \underbrace{\frac{1}{V_f} \frac{d}{dt} \left[ \Gamma_{\phi} \frac{\partial \phi_i A_{ff}}{\partial x_j} \right]}_{\text{Diffusion term}} + \underbrace{S_{\phi}}_{\text{Source term}} \quad (1)$$

Where  $\phi$  represents the solution variable to be solved, for example,  $u$ ,  $v$ ,  $w$ ,  $k$ ,  $E$  and  $\alpha_r$ .

The flow governing equations may be formed by substituting the variable  $\phi$ , the diffusion coefficient  $\Gamma_\phi$  and the source term  $S_\phi$  with the appropriate values as shown in table 1.  $V_\tau$  and  $A_\tau$  are the volume and area fractions parameters used to implement the FAVOR technique as a mean of representing the dune solid surface within the flow field. Detailed description of the implementation of FAVOR into the flow transport equations can be found in Hirt [14] and Al-Hajraf [15].

The transport equations were discretised and solved using a finite volume method for a general curvilinear coordinate system, more details of the discretization schemes and issues related to the numerical solution of the transport equations can be found in Peric [12], Iversen [13]. The standard two-equation  $k-\epsilon$  turbulent model is solved for the turbulent kinetic energy and the rate of turbulent kinetic energy dissipation.

Under the homogenous flow assumption, the particles were assumed to be small and light enough such that they follow the flow field, therefore the eddy diffusion coefficient  $\Gamma_p$  was assumed to be equal to that of the carrier phase.

Particles transported by wind usually occur in one of three modes, surface creep, saltation or suspension, Bagnold [1], Tabler [2] and Pye [3]. These processes depend upon the physical properties of the particle such as size, density and on the strength of the wind velocity component parallel to the particle bed. In this paper, models of the particle transport by saltation and suspension were considered as two separate source terms ( $S = S_{Sus} + S_{Sal}$ ) added to the particle transport equation.

### 3.1 Suspension Source term ( $S_{Sus}$ )

Considering the convection term in the transport equation for the dispersed phase flow:

$$\frac{\partial}{\partial x_j} (\alpha_p \rho u_p) = 0 \quad (2)$$

Where:  $u_p = u_{Rel} + u$  CO

Substituting (3) into (2) results in:

$$\frac{\partial}{\partial x_j} (\alpha_p \rho u_j) + \frac{\partial}{\partial x_j} (\alpha_p \rho u_{Rel}) = 0 \quad (4)$$

where the second term in the left hand side becomes the source term,  $S_{sus}$ , due to suspended particles as a function of the relative velocity and particle volume fraction.

The relative velocity can be estimated based on the *Two-Fluid model*, Ishii [5], as a function of the drag and gravitational forces:

$$|u_{Rel}| u_{Rel} = \frac{4 D_p}{3 C_D} \frac{(\rho_p - \rho) g}{\rho} \quad (5)$$

Since the particle to the air density ratio is in the order of 2000 then equation (5) can be reformed to be:

$$|u_{Rel}| u_{Rel} = \frac{4 D_p}{3 C_D} \rho_p g \quad (6)$$

Using the approximated relative velocity in (6) the suspension source term become:

$$S_{sus} = -\beta_{sus} \frac{\partial}{\partial X_j} [\alpha_p u_{Relj}] \quad (7)$$

Ishii [5] and Manninen [7] used the drift velocity derived from the Mixture theory and rewrite (7) in terms of the diffusion velocity:

$$S_{sus} = -\beta_{sus} \frac{\partial}{\partial X_j} [\alpha_p u_{Driftj}] \quad (8)$$

where the diffusion velocity is  $u_{Drift} = (1 - \alpha_p) u_{Rel}$  and  $\beta_{sus}$  is a constant that is found based on numerical experiments to be valid between 0.05 and 0.1 in flow regimes involving sand drift, Al-Hajraf [15].

### 3.2 Saltation Source term ( $S_{Sal}$ )

The saltation particle zone usually has a layer thickness of a few centimetres Bagnold [1], Pye [3]. In this layer the suspension source term is modified to take into account the saltated particles. Many authors have proposed empirical formulae to estimate the particle mass flow rate in the saltation zone based on field and wind tunnel studies, Bagnold [1], Pye [3], Iversen [13], all of which were relate the particle threshold velocity to the fluid surface shear velocity. For a quartz particle with 0.25mm diameters and 2650  $kg/m^3$  density the threshold velocity was found to be about 0.22 m/s, Bagnold [1].

In this study, the saltation source term was written in terms of particle volume fraction, the relative velocity and the dimensionless friction to threshold ratio as follows:

$$S_{sal} = R_{sal} \frac{\partial}{\partial X_j} [\alpha_p (1 - \alpha_p) u_{Relj} U_R^*] \quad (9)$$

where;

$$U_{*c} = \frac{(u_{*c}^2 + u_{*c}^2)(u_{*c}^* - u^*)}{u_{*c}^3} \quad (10)$$

$\beta_{sal}$  is a constant varies between 0.15 and 0.6, Al-Hajraf[15].

The saltation source term is applied only in the control volumes adjacent to the solid boundaries. Thus, there are three possibilities in this case for the saltation source term in individual control volumes:

1. If the friction velocity is greater than threshold value then the source term will have a negative sign and therefore an erosion process will occur.
2. If the friction velocity is equal to threshold value then the source term will be zero and neither erosion nor deposition will occur.
3. If the friction velocity is less than threshold value then the source term will have a positive sign and therefore a deposition process will occur.

It should be noted that, since the particle transport equation represents only particles of the same physical properties, particles of multiple sizes required individual transport equations to be **solved**, one for each particle size.

#### 4 Erosion/Deposition algorithm

The particle volume fraction increases or decreases as a result of the net balance between the transport terms. A control volume was assumed to be full of particles and then treated as a solid surface in the following time step if the following conditions were satisfied simultaneously:

1. If the particle phase volume fraction equals unity in a control volume, then that control volume should be treated as solid. This is difficult to achieve numerically and therefore a maximum bulk volume fraction was introduced such that if the particle volume fraction exceeded it then the control volume

was assumed to be full of particles. In the present work the maximum bulk volume fraction was assumed to be 75% of the total volume of the cell.

2. Friction velocity drops below the particle threshold velocity.

If both conditions were satisfied in a single cell then that cell was treated as a solid surface in the following calculations.

Equally a solid control volume was reopened and involved in the subsequent calculations if the friction velocity on its open face exceeded the particle threshold value. This was considered by assuming that all resisting forces were of negligible effect except the drag and the particle gravitational forces.

## 5 Results and discussions

A sand-laden flow around an identical geometry to the gate model used in the field experiment was simulated in order to obtain particle deposition patterns. The gate geometry was represented as two solid walls of 1.5m height 'H' and 20m and 15m length with a 4m gap, see figure 7. The inlet boundary was located upstream of the gate at a distance equal to 50H and the outlet boundary was 100H downstream from the wall. The side boundaries were set as a mirror boundary at 20H from the wall ends.

The domain was divided into 153 grid points in the axial direction, 75 grid points in the vertical direction and 80 grid points across the width. The distribution of these grid points took into account the requirement of finer grid resolution at areas of expected accumulation as well as around the wall and the gate where there is a significant change in the flow field as shown in figure 7.

Quartz solid particles of 250 $\mu\text{m}$  diameter and 2650  $\text{kg}/\text{m}^3$  density were used to represent the average physical properties of typical sand particles. The inlet wind profile was set based on a friction velocity equal to 0.22  $\text{m}/\text{s}$  and surface roughness equal to  $D_p/30$ . The turbulent intensity and length scale were set to be 1% and the wall height H respectively.

The different stages of the dune development at the wall sides and through the gate are shown in figure 8, where the ratio  $T/T_e$  represents the current time normalised by the time required for the deposition process to reach a steady state. Similar to those observed in the field experiment, figure 4, the dune initially started at a distance upstream from the wall where the reverse and the upstream flows meet.

The front edge of the dune formed according to the structure of the flow field, thus it is clearly shown that in the early stages a very thin layer of particles were deposited through the gate centreline. As the dune increased in size, the reverse

flow between the wall and the dune itself weakened and as a result the dune moved forward towards the wall until finally meeting it and eventually climbing the wall.

It can be seen that the dune formed in front of the long wall is larger than that formed in front of the smaller wall. This is a direct result of the ability of longer wall to reduce the flow velocity to a greater extent than the shorter wall, therefore a bigger dune developed in front of this wall.

The complex flow field immediately behind the wall and the gate is identified by the flow streamlines shown in figure 9. It is clearly shown that the flow field changed as a result of the presence of the interface solid boundary representing the dune surface. As expected, there is less disturbance of the flow field as the dune development reaches the steady state situation. This can be clarified by the streamlines in the later deposition stages where the flow streamlines passing the wall adopted a smoother shape than those passing the wall in the early stages.

Figure 10 shows the dune formed in front of the 20m wall from the upstream perspective for both field observation and numerical prediction. There is good qualitative agreement showing maximum heights of the dune at the wall centreline and minimum at the wall edges. This is a result of the flow separation at the centre of the wall and therefore a significant reduction in the flow velocity. As a consequence deposition conditions were more likely to be satisfied. The flow velocity increases when passing the wall ends, raising the friction velocity above the threshold value of the particles. Therefore the erosion conditions were satisfied and particles were unlikely to be deposited.

Due to the occurrence of the flow diffusion zone just downstream of the gate, particles were deposited forming a dune with a dome shape as shown from the field photograph in figure 6. The numerical model also captured this deposition behaviour at the same diffusion zone. Figure 11 shows the development of the diffusion zone dune from a downstream perspective. Due to the asymmetrical dimensions of the wall lengths, the dune was also shown to be of asymmetric shape at the early stages following the surrounding flow field structure. Similar to the observations, the dune then started growing in all directions, as can be seen from the dune surface ripples in figure 6 and from the surface velocity vectors in figure 11.

The model provided predictions of later stages, which have been not yet achieved in the field showing that the dune may grow and expand in all directions until the dune completely blocks the gate. In the later stages, it can be observed that two side dunes are formed within the weak flow zone created just behind the edges of the gate. These dunes grow and start to climb the downstream side of the wall, merging with the main dune and contributing to blocking the whole gate.

The last comparable behaviour that was captured by the model and clearly demonstrated in the field observation is the strong erosion area near the wall resulting from the acceleration of the flow as it passes through the gate, figure 5. Comparison of this photograph with the prediction at  $T/Te = 10\%$  in figure 11, shows the erosion zones at the sides of the gate are clearly captured by the model wherever a high wind velocity occurs.

## 6 Conclusion

A numerical model based on the homogenous two-phase theory was introduced to simulate air-sand flow and sand accumulation around a three-dimensional gate. The numerical model was employed to predict the transport, erosion and deposition processes of sand particles around obstacles. The model is largely independent of empirical expressions used to estimate the particle mass flow rate, which play an essential role the deposition erosion processes. The model shows a good qualitative agreement with the field observations especially at the early deposition **stages**, at which the shape and location of the initial depositions were captured successfully.

In conclusion, a practical CFD tool has been developed and validated, incorporating novel physical and numerical models. The tool can be utilised by scientists and engineers to further understand the real world problem of drifting sand and snow in urban and industrial environments.

## 7 References

- [1] Bagnold, R.A. *The physics of blown sand and desert dunes*. London: Methuen, 1941.
- [2] Tabler, R.D. *Design guidelines for the control of blowing and drifting snow*. Washington: National Research Council, 1994.
- [3] Pye, K. & H. Tsoar, *Aeolian Sand and Sand Dunes*. London: Unwin Hyman, 1990.
- [4] Iversen, J. D. Comparison of wind tunnel model and full-scale snow fence drifts, *J. WindEng. Ind. Aerodyn.* 8, pp. 231-249, 1981.
- [5] Ishii, M. *Thermo-fluid dynamic theory of two-phase flow*. Eyrolles, 1975.

- [6] Gosman, A.D. Developments in CFD for industrial and environmental applications in wind engineering, *J. Wind Eng. Ind. Aerodyn.* 81, pp. 21-39, 1999.
- [7] Manninen, Mikko, Veikko Taivassalo & Sirpa Kallio, *On the mixture model for multiphase flow*, VTT-288 Publications, Finland: Technical Research Centre of Finland, 1996.
- [8] Kawamura, T., Kan Makiko & Hayashi Tsutomu, Numerical study of the flow and the sand movement around a circular cylinder standing on the sand, *JSME International Journal*, 42(4), pp.05-611, 1999.
- [9] Uematsu, T., T. Nakata, K. Takeuchi, Y. Arisawa & Y. Kaneda, Three-dimensional numerical simulation of snowdrift, *Cold Region Science and Technology*, 20, pp.65-73, 1991.
- [10] Sundsbø, Pre-Arne. *Numerical modelling and simulation of snow drift*, PhD. Thesis, Norway: ISBN 82-471-0047-9, 1997.
- [11] Wipperman, F.K. & G. Gross, The wind induced shaping and migration of an isolated dune - A numerical experiment, *Boundary-Layer Meteorology*, 36 pp.319-334, 1986.
- [12] Peric, M. *Finite volume method for the prediction of three-dimensional fluid flow in complex duct*, PhD. Thesis, London: Imperial College, 1985.
- [13] Iversen, J. D. & Keld R. Rasmussen . The effect of wind speed and bed slope on sand transport. *Sedimentology*, 46, pp.723-731, 1999.
- [14] Hirt, C. W. Volume-Fraction Techniques: Powerful Tools for Wind Engineering. *J. Wind Eng. Ind. Aerodyn.* 47, pp.327-38, 1993.
- [15] Alhajraf, S. *Numerical two-phase flow modelling of drifting sand*, PhD. Thesis, Cranfield University, (2000) - Under preparation.
- [16] Kwarteng, A.Y., V. Singhroy, R. Saint-Jean, and D. Al-Ajmi. 1997. RADARSAT SAR data assessment of the oil lakes in the Greater Burgan oil field, Kuwait. *Proceedings, International Symposium on Geomatics in the Era of RADARSAT*, Ottawa, Canada, May 24-30.

Table 1: Formulation of the general transport equation variables

	$\phi$	Diffusion Coeff. $\Gamma_\phi$	Source Term $S_\phi$
Continuity	1	0	0
x-momentum	U	$\Gamma_u$	$-\frac{\partial P}{\partial x} + S_u$
y-momentum	V	$\Gamma_v$	$-\frac{\partial P}{\partial y} + S_v$
z-momentum	W	$\Gamma_w$	$-\frac{\partial P}{\partial z} + S_w$
Kinetic energy	$k$	$\frac{\mu_T}{A^*}$	$\tau_{ij} \frac{\partial U_i}{\partial X_j} - \epsilon$
Kinetic energy dissipation	e	$\frac{\mu_T}{\sigma_\epsilon}$	$C_{1,\epsilon} \frac{\epsilon}{k} \left( \tau \frac{\partial U_i}{\partial X_j} \right) C_{2,\epsilon} \rho \frac{\epsilon}{k}$
Particle volume fraction	$\alpha_p$	$\Gamma_p$	$S_p = S_{Susp.} + S_{Salt.}$

Where:

$C_\mu$	$C_{1,\epsilon}$	$C_{2,\epsilon}$	$\sigma_k$	$\sigma_\epsilon$
0.09	1.44	1.92	1.0	1.3

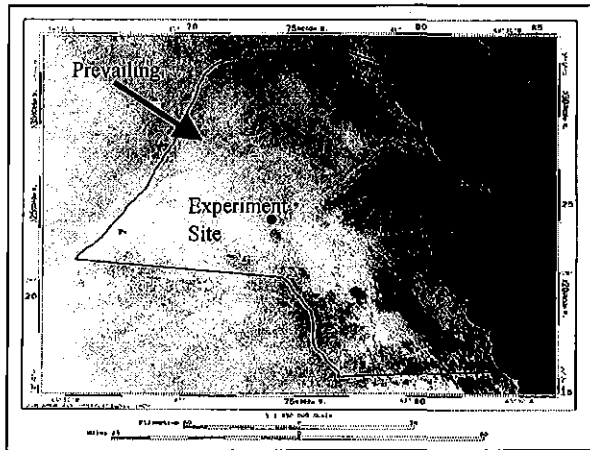


Figure 1: Landsat satellite image of the State of Kuwait showing areas under an active mobile sand sheet. After Kwarteng [16].

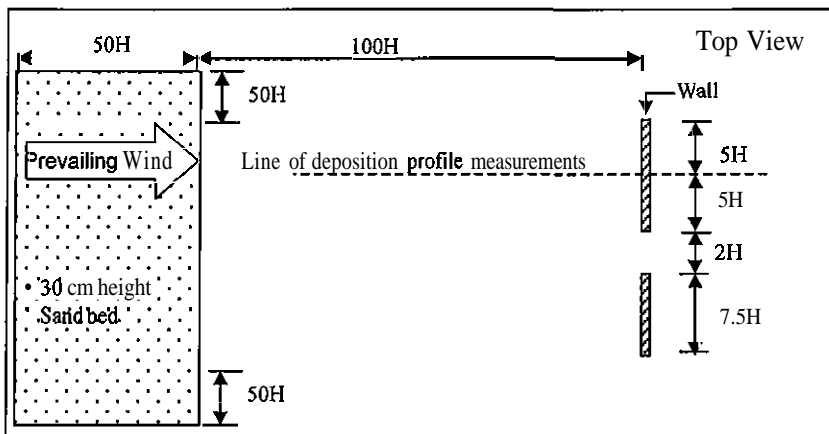


Figure 2: Geometry of the gate field experiment at the Kuwait desert July 1999. The wall height  $H = 1.5\text{m}$ .

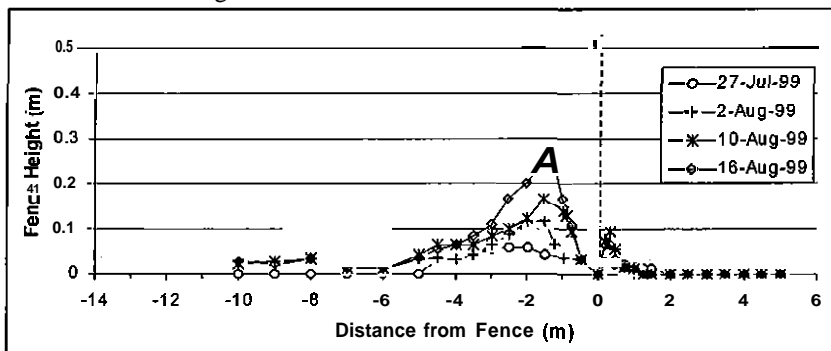


Figure 3: Four stages of the deposition profile at the middle of the 20m wall in the gate simulation experiment.

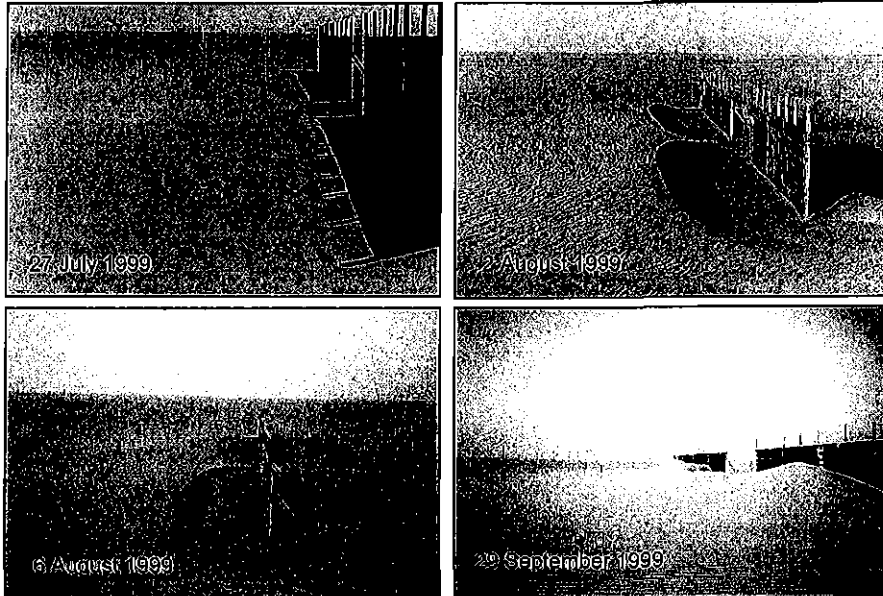


Figure 4: Four stages of the deposition process around simulated gate at Jahra site.

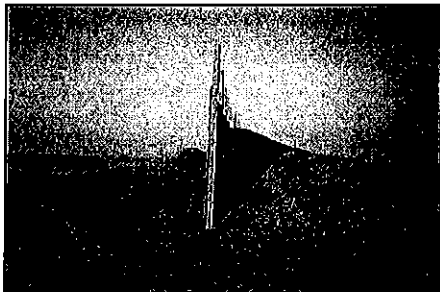


Figure 5: Side view showing erosion at high wind velocity areas and deposition at reverse flow zones. Photograph at September 1999.

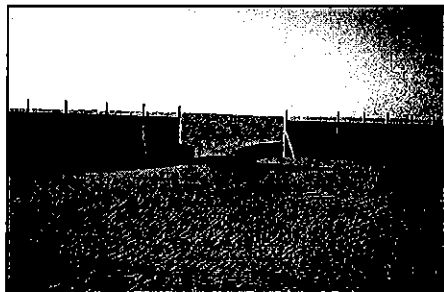


Figure 6: Front view showing the diffusion zone downstream the gate. Photograph at September 1999.

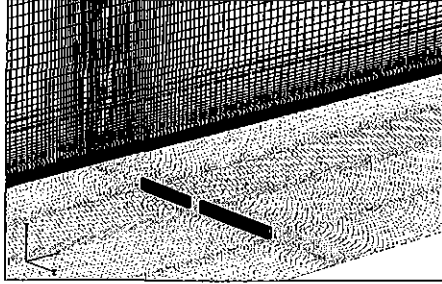


Figure 7: Computational domain showing the gate and wall geometry with the grid distribution.

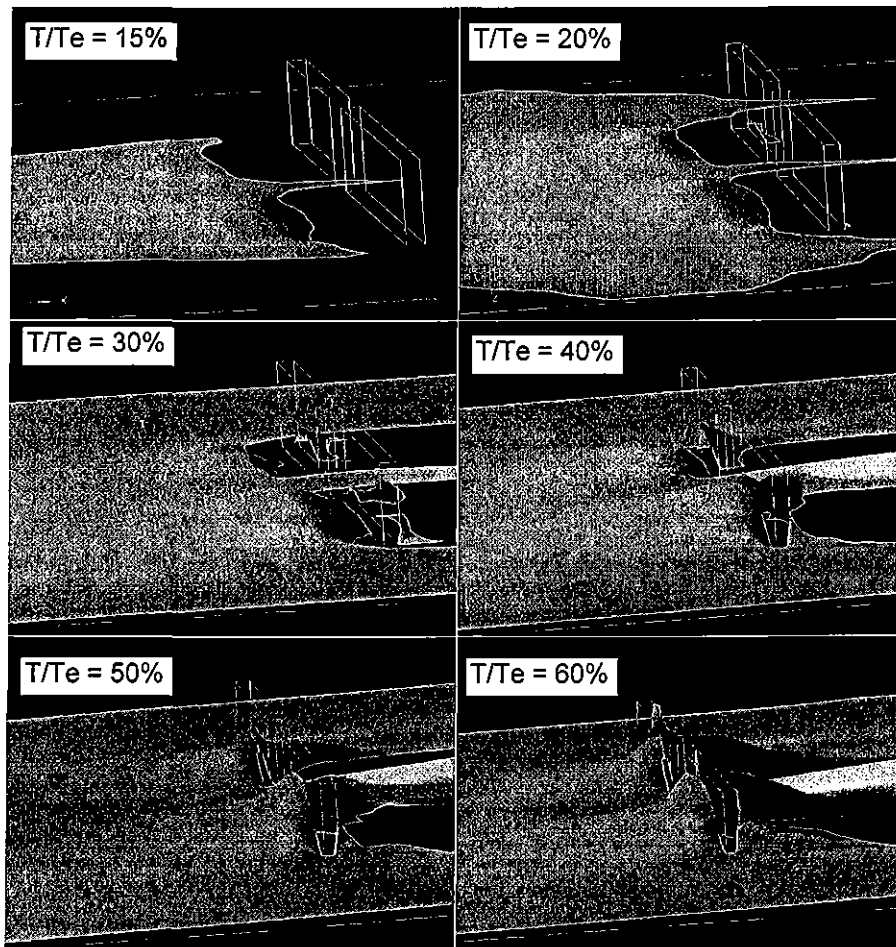


Figure 8: **Simulation** of the deposition stages around an open gate using the Homogenous model coupled with FAVOR. Isosurface of volume fraction at 0.75. The colour shading for illustration purposes only.

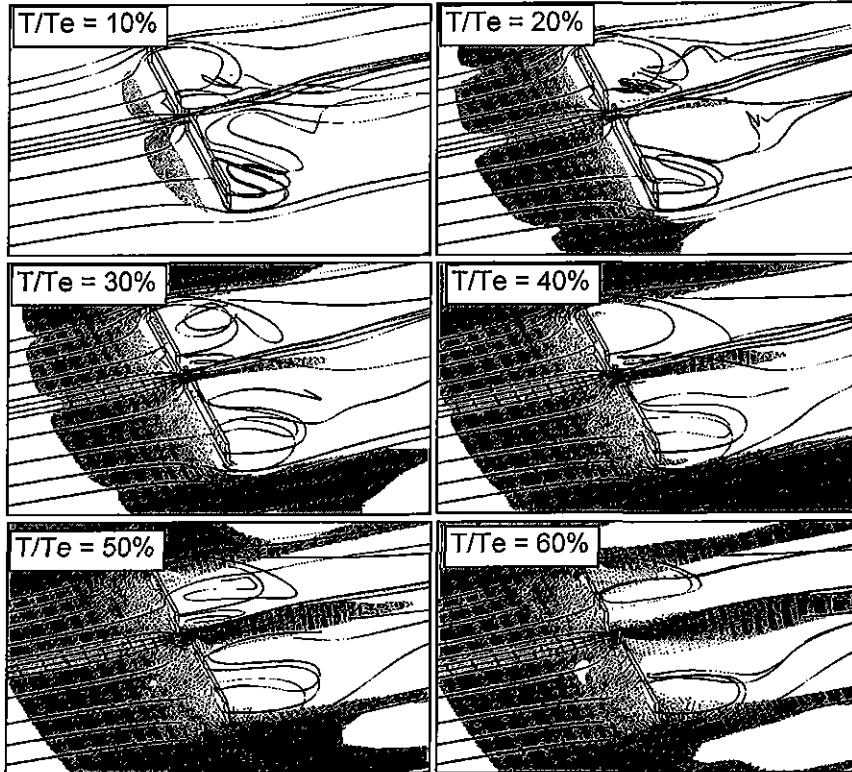


Figure 9: Deposition stages around open gate showing the effect of the interface boundary on the flow field represented by surface velocity vector and flow streamlines. Isosurface of volume fraction at 0.75. The colour shading for illustration purposes only.

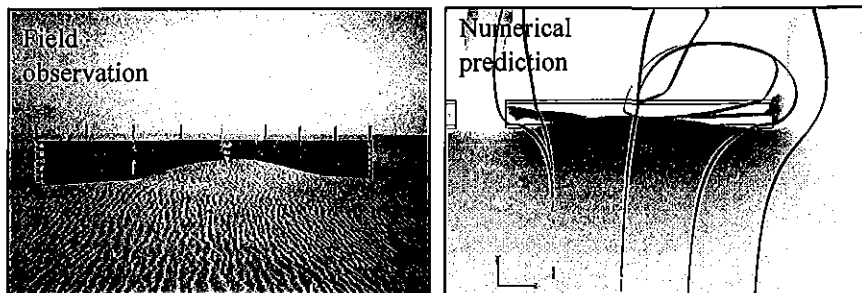


Figure 10: Upstream view of the deposition in front of the 20 m wall. Isosurface of volume fraction at 0.75.

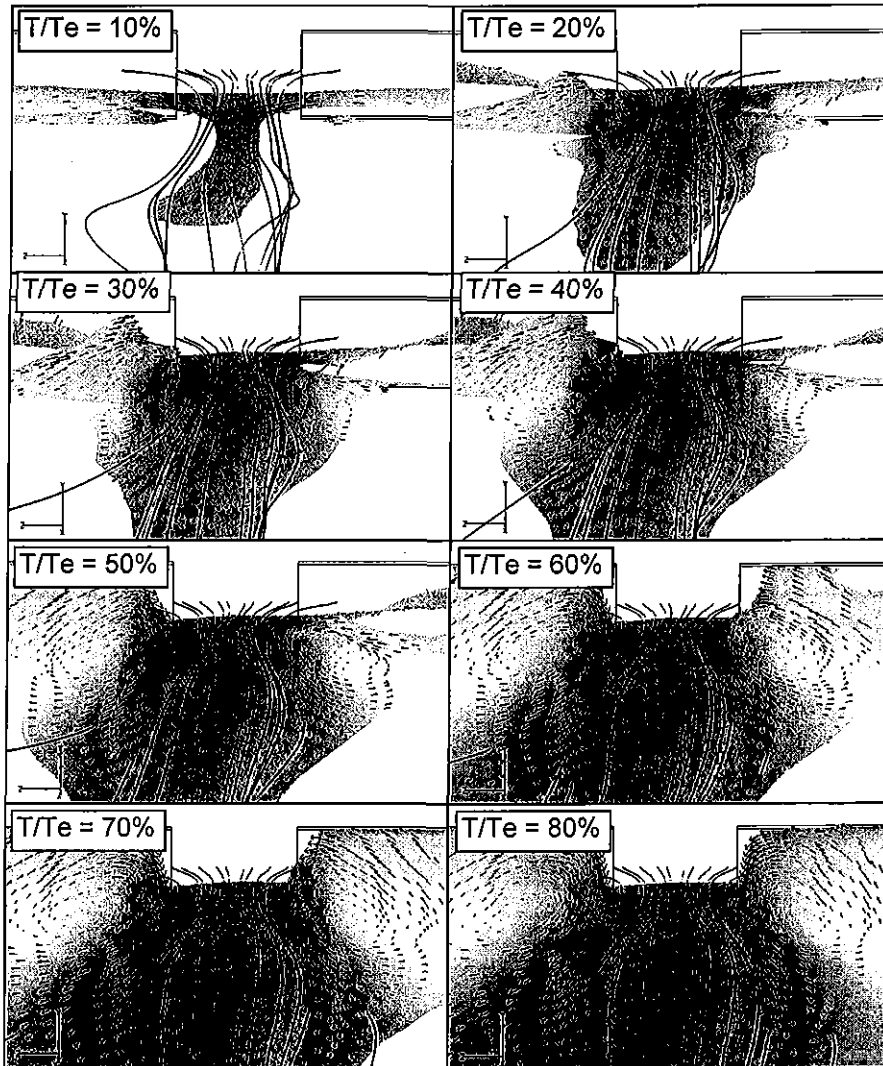


Figure 11: The Development stages of the diffusion dune downstream the gate showing the surface velocity vector and flow streamlines. Isosurface of volume fraction at 0.75.